Hyperspectral Image Turbulence Measurements of the Atmosphere

Sarah E. Lane[a], Leanne L. West[a], Gary G. Gimmestad[a],
Stanislav Kireev [b], William L. Smith, Sr.[b], Edward M. Burdette[a],
Taumi Daniels[b], and Larry Cornman[c]
[a]Georgia Tech Research Institute, Atlanta, GA 30332
[b]Hampton University, Hampton, VA 23668
[c]University Corporation for Atmospheric Research, Boulder, CO 80307

ABSTRACT

A Forward Looking Interferometer (FLI) sensor has the potential to be used as a means of detecting aviation hazards in flight. One of these hazards is mountain wave turbulence. The results from a data acquisition activity at the University of Colorado's Mountain Research Station will be presented here. Hyperspectral datacubes from a Telops Hyper-Cam are being studied to determine if evidence of a turbulent event can be identified in the data. These data are then being compared with D&P TurboFT data, which are collected at a much higher time resolution and broader spectrum.

Keywords: hyperspectral image processing, standoff gas detection, remote sensing, aviation safety

1. INTRODUCTION

The real-time detection of atmospheric turbulence is of great interest due to the applicability to aviation safety. A FLI sensor has the potential to be used as a means of detecting aviation hazards in flight, giving the flight crew time to react. One of these hazards is mountain wave turbulence. Mountain waves are often associated with the presence of lenticular clouds, which pilots will avoid, and normally persist all day, so that pilot reports (PIREPS) can be used to avoid areas of moderate to severe turbulence. However, there have been reports[1] of unexpected encounters with mountain waves and turbulence that have resulted in damage to aircraft, injury, and loss of life that make the capability of real-time detection of these events desirable.

The results from a data acquisition activity at the Mountain Research Station near Boulder, Colorado during November of 2011 are presented here. This site experiences mountain waves and mountain wave turbulence in the fall and winter months, which affect flights into Denver International Airport. The two main objectives of this test were as follows:

- Observe slowly-varying radiance patterns associated with standing waves.
- Observe short-term fluctuations associated with turbulence.

These objectives require that long data sets (approximately thirty minutes) at as high as possible temporal resolution be collected of the sky by interferometric means. This collection activity utilized both a long wave infrared Telops Hyper-Cam and a Designs and Prototypes (D&P) TurboFT spectrometer, both operating in continuous mode simultaneously for approximately thirty minutes for each data collection event. Each sensor provides unique information about the sky; the Hyper-Cam collects LWIR hyperspectral image data of the scene, while the TurboFT has the capability to collect approximately 100 spectra per second in the 2.5-16 micron region. Both sensors have on-board blackbodies, which allow for calibrated radiance in the field. The two sensors were co-located on a custom built mount which allowed bore-sighting of the sensors for the test so that they would be observing the same area of sky throughout each measurement period.

The Hyper-Cam data addressed the first objective in that the long data sets could capture slowly-varying radiance, while the TurboFT data addressed the second objective in that the high temporal resolution and broader spectrum could capture short-term fluctuations. Both datasets are being investigated as a means of studying the feasibility of using a FLI sensor for the detection of turbulent events; this paper presents preliminary results from these data.

2. DATA COLLECTION ACTIVITY

2.1 Mountain Research Station Test Site

The Mountain Research Station (MRS) is located on the front range of the Rocky Mountains at an elevation of 2,900 m (9,500 ft), approximately 76 km (47 mi) WNW of Denver International Airport. This elevation and clear line of sight towards the airport makes the Mountain Research Station an ideal location for observing mountain waves that form over the Rockies.

Several sites at elevations higher than the main lab were selected for possible locations for the data collection; however, due to snow cover and an in-operational Sno-Cat, the data collection was confined to the dining hall and parking lot at the Mountain Research Station. However, this did not inhibit the data collection; even though the instruments were below the tree line, looking out of an open window from the second floor of the dining hall provided a clear view of the sky over the trees in the direction of Denver (shown in Figure 1).

Figure 1. Instrument set-up looking out the open window of the MRS dining hall (*left*), and instruments looking ESE toward Denver (*right*).

2.2 Hyper-Cam Settings

The Telops Hyper-Cam is a long-wave infrared hyperspectral imaging sensor[2] with variable resolution from 0.25 – 150 cm^{-1} and a variable image size of up to 320 x 256 pixels. The data it provides is referred to as a datacube; the three dimensions of data are (x, y, σ), where x and y are spatial information (i.e., the pixel in an image), and σ is the spectral information (i.e., radiance at wavenumber σ). Therefore, each datacube is composed of a radiance image at narrow wavebands within the LW portion of the spectrum.

The entire 320 x 256 window was used, and for the majority of the test, the Hyper-Cam was operated with a 0.25X magnification lens, which increased the field of view from 6.4° horizontal x 5.1° vertical FOV to 25.6° horizontal x 20.4° vertical FOV. However, for the runs discussed in this paper, the smaller field of view was used. In these tests the spectral resolution was set at 16 cm^{-1}. Sixteen wavenumber datacubes contain 41 frames in the spectral dimension between 810.06 and 1341.24 cm^{-1}; each is collected in approximately 1696 ms with a 65 ms delay between each cube.

This wavenumber resolution was chosen because previous models showed collection at 16 cm^{-1} resolution provides the highest temporal resolution while still capturing enough spectral information to distinguish a turbulent wave event[3]. The recording frequency of the Hyper-Cam instrument is not high enough to capture a turbulent event; however the spatial information it provides over 30 minutes could make it possible to visually detect the location of standing waves. This information can then be used to isolate certain time periods of TurboFT spectra for analysis.

2.3 TurboFT Settings

A Designs and Prototypes (D&P) TurboFT spectrometer was used simultaneously with the Hyper-Cam to provide spectral data at higher temporal resolution. The D&P TurboFT is a dual InSb/MCT detector instrument capable of providing up to 100 spectra per second from 2.5 to 16 μm. For this data collection activity, spectra were collected at 4 cm^{-1} resolution and set at four coadds, which corresponds to four interferograms being averaged to produce each spectrum. These settings resulted in a recording rate of 12 spectra per second. This higher temporal resolution than that of the Hyper-Cam allows for a better chance for observation of short-term fluctuations associated with turbulence.

The TurboFT sensor was equipped with a four inch telescope which provided a 1.2 degree field of view. It was determined early in test planning that the TurboFT 1.2 degree FOV must be aligned with the center of the Hyper-Cam FOV. A common mount that allowed for bore-sighting of the sensors, as well as protected the TurboFT from the elements, was developed and is explained in the next section.

2.4 Sensor Mount

The Hyper-Cam was not expected to have any issues with the lower temperatures expected in Colorado in November, however, the safe operation of the TurboFT required that an enclosure be built for it that would provide a stable thermal environment. An aluminum box was constructed to house the TurboFT; a heater was placed inside, and the enclosure was insulated. A mount for both the Hyper-Cam and the TurboFT enclosure was then constructed from unistrut that would allow both the Hyper-Cam and TurboFT enclosure to be mounted via dovetail slides. The mount was constructed such that both sensors could be rotated from 90 to zero zenith angle viewing geometry while maintaining bore-sight (it should be noted that the mount was never rotated to the zero zenith angle position with the D&P installed to avoid damage to the sensor). A SolidWorks representation of the mount with both Hyper-Cam and D&P installed is shown in Figure 2.

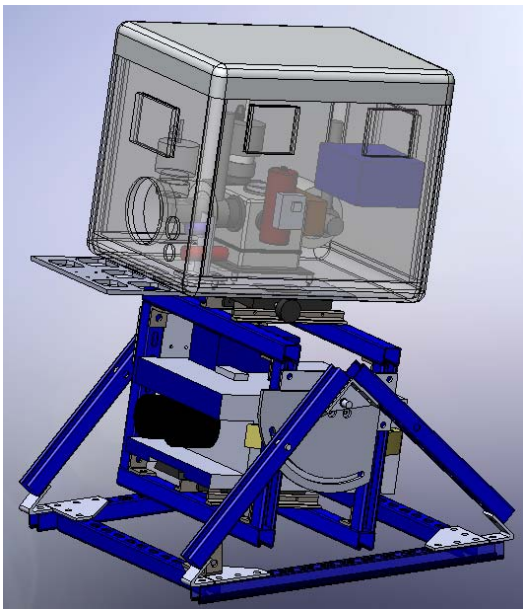

Figure 2. A SolidWorks representation of the bore-sight mount with TurboFT in aluminum enclosure (*top*) and Hyper-Cam (*bottom*).

Alignment of the center of the TurboFT FOV with the center pixel of the Hyper-Cam image was tested after a complete tear-down and reassembly of the sensor mount both before and during the field test.

2.5 Ancillary Data

During this test, the only ground truth data that exists to identify a turbulent event is from pilot reports (PIREPS) and Eddy Dissipation Rate (EDR) reports. During this test, PIREPS were continuously monitored by team members in the

event that any severe turbulence was reported in the area of MRS; instruments could then be directed toward the location of the PIREP. However, during the time of the test, only moderate turbulence was reported. Full PIREP and EDR reports were compiled after the test. Meteorological data, including temperature, humidity, pressure, wind speed, and solar radiation data, was provided by MRS personnel for the dates of the test from a weather station at MRS's C1 site, located 0.78 km (0.49 mi) from the test site at 3,022 m (9,912 ft) elevation.

The Hyper-Cam comes equipped with a visible camera; however, a webcam was used instead to record visible imagery of the sky. While the webcam has a much wider field of view than either the Hyper-Cam or the TurboFT, it provided visible documentation of any obscurations to a clear field of view, such as clouds, aircraft, or aircraft contrails. The webcam was placed inside the TurboFT enclosure so that it too would be bore-sighted with all other instruments.

3. METHODOLOGY AND PRELIMINARY RESULTS

Each thirty minute data collection event produced approximately 1,000 Hyper-Cam datacubes and 20,000 TurboFT spectra. The Hyper-Cam data were investigated first in order to find visual cues to locations of possible waves or turbulence. Results from the fourth dataset from November 17, 2011 will be shown here. For this dataset, a large lenticular cloud was in the scene and the instruments were lined up to view the area right under the cloud, at 112° azimuth and 4° elevation viewing angle. Figure 3 shows the viewing geometry as recorded by the webcam.

Figure 3. A visible image of the viewing geometry for the fourth dataset collected on Nov. 17, 2011. The red box shows the approximate Hyper-Cam field of view.

3.1 Datacube Reduction

The series of datacubes produced a four dimensional dataset (x, y, σ, t). x, y, and σ comprise the dimensions of the original datacube; t is the time element. Variability in the time series of datacubes was investigated first, and was tested only at one spectral location in the datacube at a time. A reduced datacube was created with spatial and time dimensions only (x, y, t) for spectral locations of interest. The following criteria were considered when choosing spectral locations from the original Hyper-Cam data for processing in the reduced datacubes:

- Choose locations in the spectral domain where any variability can be considered true variability and not due to noise (i.e., not at the extremes of the spectral range of the Hyper-Cam, where the NESR is higher and noise is more prominent in the spectrum than signal).
- Choose locations which correspond to water vapor lines, because previous models[3] have demonstrated that temperature and moisture variations at these lines could be exploited for detection of waves and turbulence.

The reduced (x, y, t) datacubes were then corrected for bad pixels in order to avoid bad values creating unrealistically high variability. This was done by applying a spatial filter to each image, whereby each pixel was compared to the average of the neighboring eight pixels, and if the absolute value of the difference was greater than one standard deviation of the neighbors, the pixel was replaced with the average. Due to the small neighborhood of surrounding pixels, there were still some areas of each image that showed high spatial variability, and so a median filter was applied to smooth the images.

3.2 Datacube Differencing by Subtraction of the Mean

After the filtering was applied to each image in the reduced datacube, the mean radiance value at each pixel index for all times was calculated. This created a mean image which was then subtracted from each image in the reduced datacube, creating a "difference cube". Each image from the difference cube was then strung together to create a movie file showing the time evolution of variability. See below for the video (linked in online version) for a run from November 17, 2011, showing the time evolution of variability in radiance at 956.13cm^{-1}. This wavenumber was chosen because models showed it exhibited the highest variability[3].

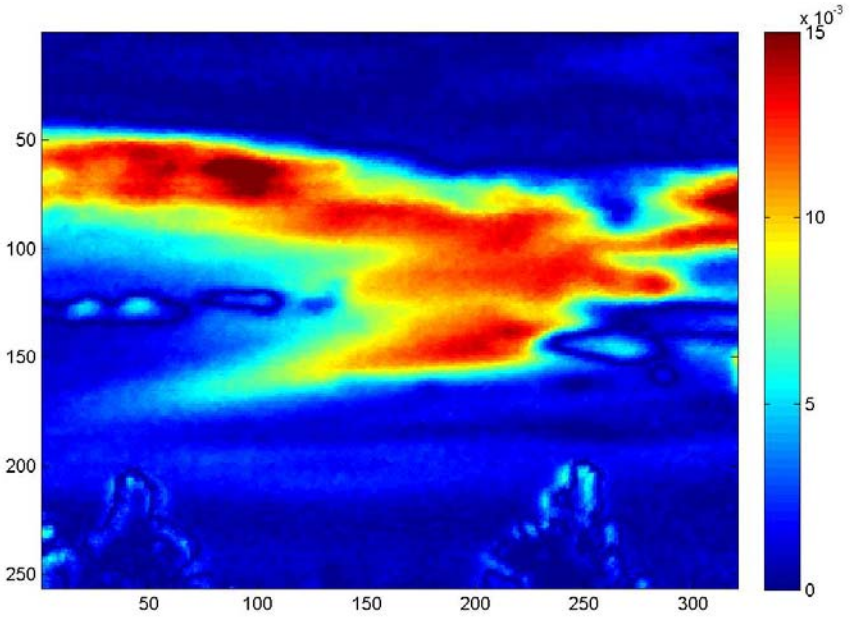

Video 1. "VariabilityMovie1.wmv", which shows the time evolution of radiance variability in the sky scene under the lenticular cloud. http://dx/doi.org/doi.number.goes.here

3.3 Cloud Removal

The video file shows that there are areas of high variability in the area under the lenticular cloud; however, comparison with the visible imagery from the webcam indicated that this could be due to higher radiance of incoming clouds at the end of the time series. By exploiting the spectral nature of the Hyper-Cam datacubes, a simple test was developed to classify clear sky or clouds.

The sky is the coldest object in these scenes, more so than clouds, treetops, or any other obscuration. A comparison of sky radiance vs. cloud radiance is shown in Figure 4.

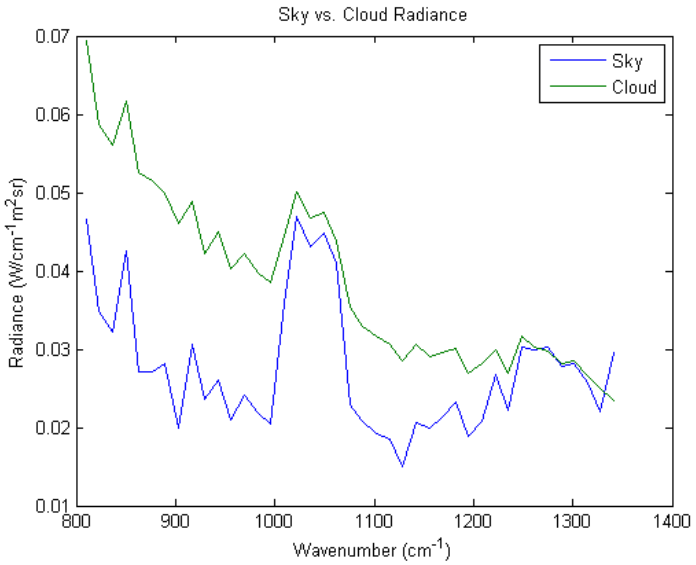

Figure 4. The radiance from a sky pixel compared to the radiance from a cloud pixel.

The spectra shown in Figure 4 are from the same row of pixels so that the elevation angle for both would be the same and not create a difference in magnitude. These spectra are at 16 cm^{-1} resolution, so the narrow spectral lines characteristic of a sky spectrum cannot be seen in the measured sky radiance; however, there is enough difference in the two spectra so that a determination of sky or "other" can be made for every pixel in the scene. The cloud spectrum exhibits much higher radiance than the sky spectrum; additionally it has fewer spectral features and follows more closely the trend of a blackbody.

In order to determine the areas of clear sky, the following procedure was followed. Frame 8 (903.02 cm^{-1}) from each datacube in time was chosen to be the frame that exhibited a substantial difference between sky and cloud spectra. Frame 35 (1261.67 cm^{-1}) from each datacube in time was chosen to be the frame that exhibited the most similarity between sky and cloud spectra. For every time in the series, frame 35 was subtracted from frame 8. A binary image was created for every time step, whereby if the result of the subtraction was positive, a one was assigned to the pixel, and if the result of the subtraction was negative, a zero was assigned to the pixel. By overlaying these binary images over the difference images described in the previous section, everything but clear sky should be masked, which helps in the determination of whether variability can be attributed to temporal changes in cloud position. Variability images from the beginning and end of the time series, both unmasked and masked, are shown in Figure 5.

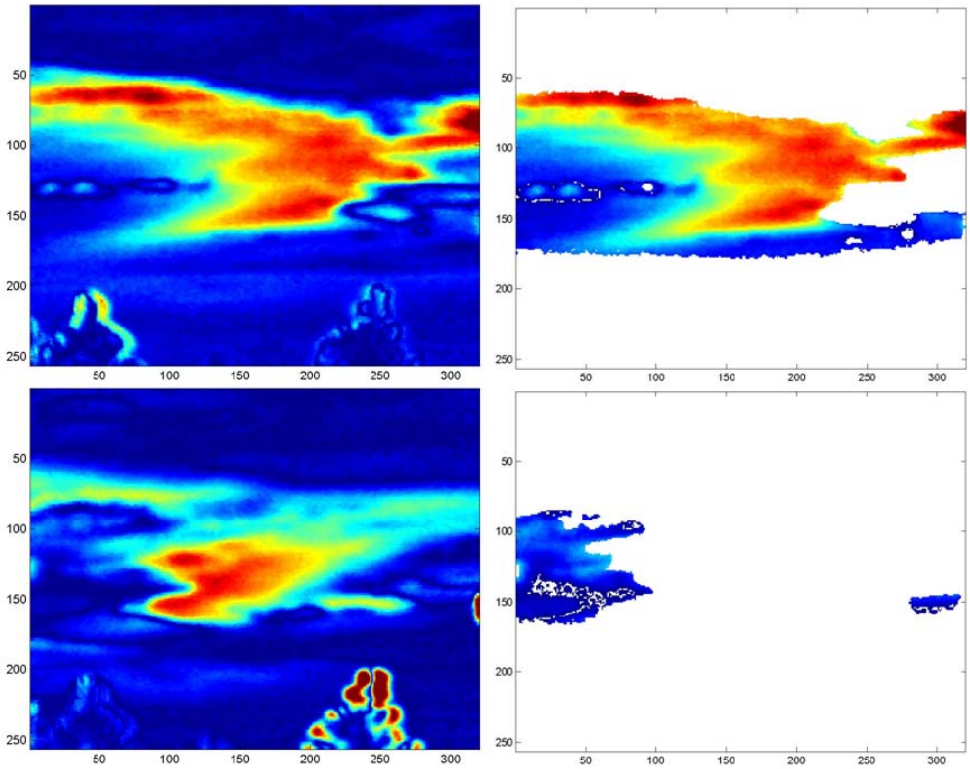

Figure 5. The variance in radiance at the beginning of the thirty minute run (*top two images*) vs. the variance in radiance at the end of the thirty minute run (*bottom two images*). The images on the right have been masked by the cloud removal test.

Figure 5 demonstrates that this simple algorithm to test for sky also masks clear sky at the horizon as the atmosphere here is more opaque and its radiance looks more like a blackbody. Therefore, a second test was developed that would compare the relative change in radiance between frame 8 (903.02 cm^{-1}) and frame 9 (916.30 cm^{-1}). As shown in Figure 6, both sky spectra, regardless of elevation angle, exhibit a much greater change between the two wavenumbers than the cloud spectrum.

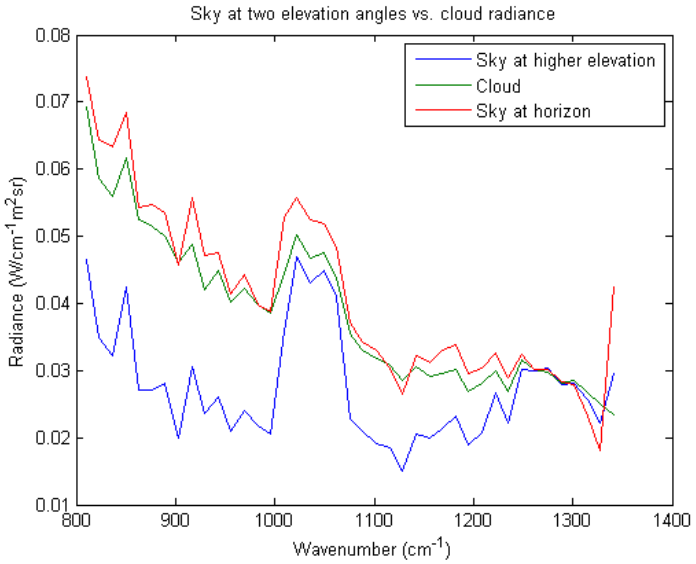

Figure 6. The radiance from sky pixels at two elevations compared to the radiance of a cloud pixel.

The relative difference of the local radiance between 903.02 cm^{-1} and 916.30 cm^{-1} of the three spectra in Figure 6 is 8.133 x 10^{-4} W/m^2sr in the case of the sky at the high elevation, 2.410 x 10^{-4} W/m^2sr in the case of the cloud, and 7.681 x 10^{-4} W/m^2sr in the case of the sky at the horizon. Because the sky radiance changes approximately three times faster in the case of both sky spectra, this derivative is checked in addition to the radiance difference between 903.02 cm^{-1} and 1261.67 cm^{-1}. Variability images from the beginning and end of the time series, both unmasked and masked with the new constraint are shown in Figure 7. These images are from the same time as those shown in Figure 5.

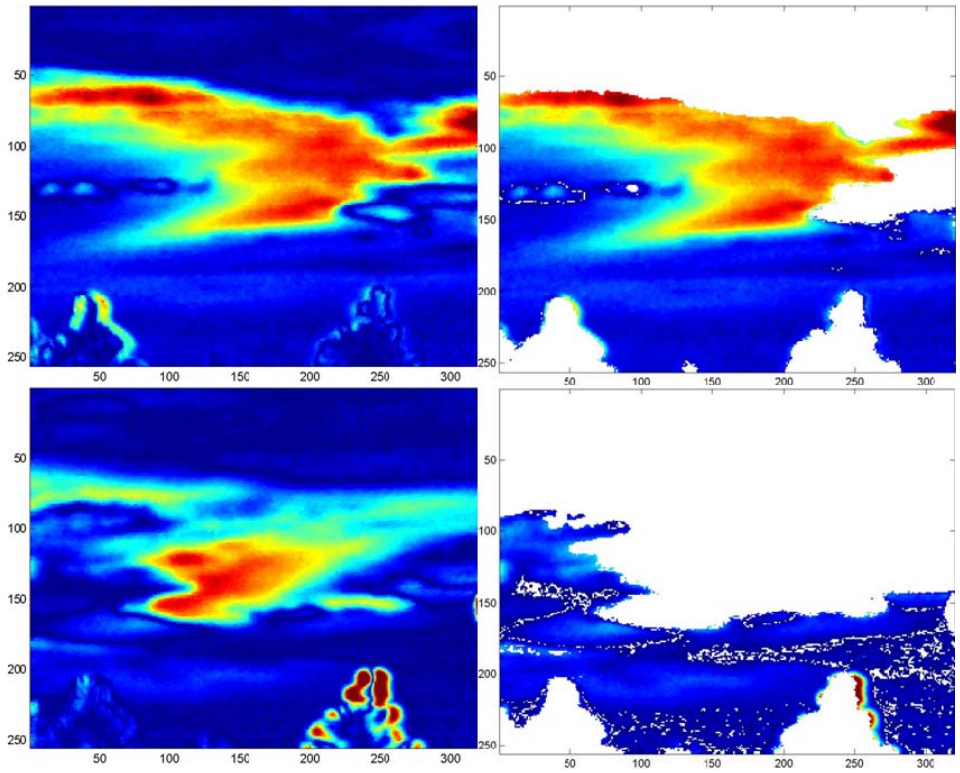

Figure 7. The variance in radiance at the beginning of the thirty minute run (*top two images*) vs. the variance in radiance at the end of the thirty minute run (*bottom two images*). The images on the right have been masked by the cloud removal test as in Figure 5, but with the additional constraint of checking the change in radiance between 903.02 cm^{-1} and 916.30 cm^{-1}.

3.4 Datacube Differencing Using Rank Order Statistics

Applying the cloud mask showed that the appearance of clouds in the scene later in the time series was significantly contributing to the variability as the higher radiance of the clouds was affecting the mean. Therefore, instead of calculating the mean radiance of each pixel for the entire time series, the radiances of each pixel were ranked in ascending order prior to calculating a mean. Every pixel in the time series was sorted by ascending radiance; the higher radiances that can be attributed to clouds are therefore all located in the higher quantiles and can be excluded from analysis.

The upper and lower bounds for which to calculate an average radiance were chosen somewhat arbitrarily. The median values were found for every pixel and then this was subtracted from each image in the reduced datacube (x, y, t). Additionally, because the high radiance values are unwanted, an average was calculated from the ranked data between zero and 50%. This average was then subtracted from each image in the reduced datacube. These results were then compiled into a movie with the cloud mask applied; this can be seen in the following video.

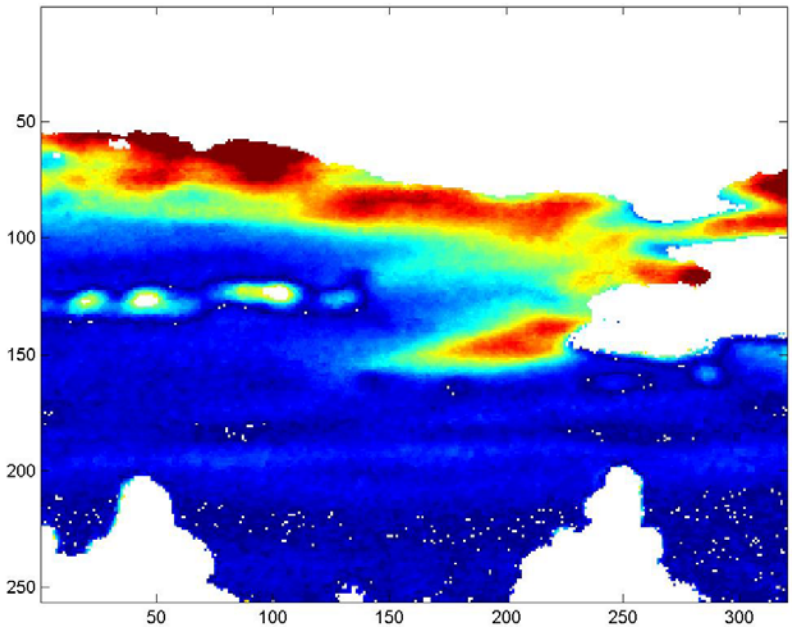

Video 2. "VariabilityMovie2.wmv", which shows the time evolution of radiance variability calculated from an average that includes only the first 50% of ranked radiance data. http://dx/doi.org/doi.number.goes.here

The mean that is calculated to create the variability seen in Video 2 should not have as much cloud influence; however, the clouds affecting the mean still cannot be excluded.

4. FUTURE WORK

Analysis up to this point has only focused on visual examination of time evolution of variability in Hyper-Cam data. Because turbulence is associated with temperature and moisture variations, it could be possible to exploit the spectral domain of the datacubes by comparing measured radiance to water vapor spectra, modeled at different temperatures and concentrations, using standard gas detection algorithms. The authors have investigated these algorithms previously[4] as they apply to the detection of aircraft exhaust.

In addition investigating gas detection algorithms for hyperspectral data, the authors plan to begin analysis of the TurboFT data. This high temporal resolution spectral data will be analyzed to see if short term fluctuations in radiance can be identified in the time series. This could potentially indicate turbulent events. If fluctuations in the TurboFT data are identified, these times will then be compared to the Hyper-Cam hyperspectral imagery. Similarly, if standing waves are identified in the Hyper-Cam data, these times will then be compared to corresponding time sequences in D&P data.

5. CONCLUSIONS

This paper discussed preliminary results from a data collection at Mountain Research Station near Boulder, Colorado in November of 2011. As of this writing, only the Hyper-Cam datacubes have been investigated. The visual inspection of the time evolution of variability has been used as the main metric for determining where in the field of view standing waves or turbulence is most likely. Further analysis is needed for a conclusive determination on whether or not the turbulent events can be identified in these data; however, results thus far indicate that this identification could be possible.

ACKNOWLEDGEMENTS

The research described here was funded by the NASA Aeronautics Research Mission Directorate (ARMD) Aviation Safety (AvSafe) Program, under the Atmospheric Hazard Sensing & Mitigation (AHSM) area within the Atmospheric Environment Safety Technologies (AEST) project.

The authors wish to thank Jack Wood of GTRI for designing and constructing the D&P enclosure and boresight mount, Kelly Matheson and Jennifer Morse of Mountain Research Station for providing access to and testing assistance at MRS, and Julie Prestopnik of UCAR for compiling EDR and PIREP reports.

REFERENCES

[1] West, L., Gimmestad, G., Smith, W., Kireev, S., Cornman, L. B., Schaffner, P. R., Tsoucalas, G., "Applications of a Forward-Looking Interferometer for the on-board detection of aviation weather hazards," NASA/TP-2008-215536; Added to NTRS: 2008-12-10; Document ID: 20080045836; Report Number: L-19522.

[2] Farley V., Vallières, A., Chamberland, M., Villemaire, A., and Legault, J-F. "Performance of FIRST, a longwave infrared hyperspectral imaging sensor," Proc. SPIE 6398 (2006).

[3] West, L., Gimmestad, G., Smith, W., Kireev, S., Daniels, T., Cornman, L., "Airborne Forward Looking Interferometer for the Detection of Terminal-Area Hazards," NASA Contract NNX09AR67A Annual Report, Year 2 (July 2011).

[4] Lane, S. E., West, L. L., Gimmestad, G. G., Smith, W. L., and Burdette, E. M., "Detection of aircraft exhaust in hyperspectral image data," Proc. SPIE 8158 (2011).